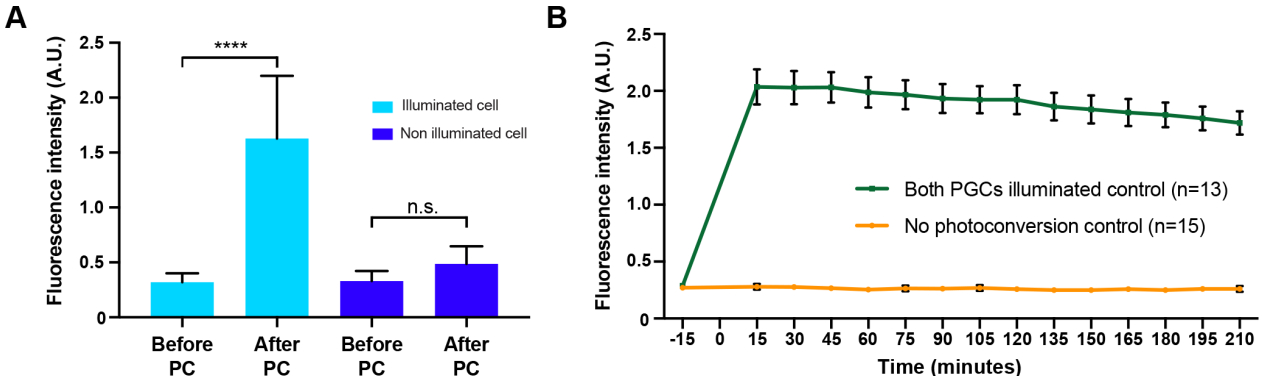

Fig. S1. (A) Mean levels of photoconverted Dendra2 fluorescence intensity measured before and immediately after photoconversion (PC) in the illuminated (light blue) and non-illuminated (dark blue) regions of the PGCs that are defined in Figure 1F. Dendra2 photoconversion in one cell (light blue) does not significantly impact fluorescence levels in the other cell (dark blue). Error bars are standard error of the mean, n = 13 animals. Statistical analyses were done using a one-way ANOVA test with a Tukey *post hoc* test (ns = not significant, p = 0.55, **** = p < 0.0001). (B) Mean levels of photoconverted Dendra2 fluorescence intensity measured over time (in seconds) when the entire primordial germ line is illuminated by the photoconverting laser at time 0 (green line, n = 15) or when no photoconverting laser illumination is performed (orange line, n = 13). Error bars are standard error of the mean.

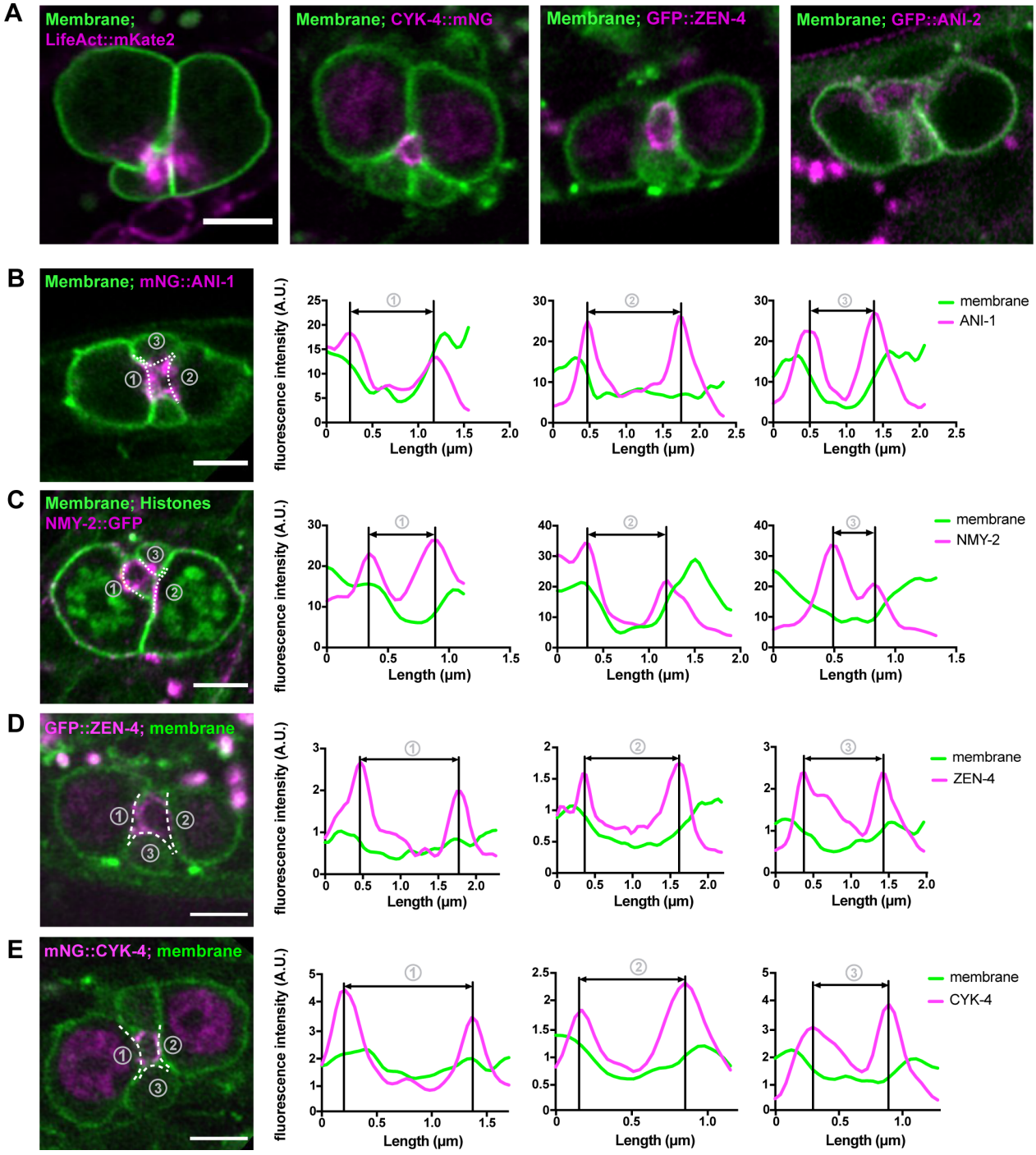

Fig. S2. (A) Confocal images (sum projection of 3 slices) of the PGCs in first larval stage animals expressing FP-tagged markers for membrane (mCh-PH$^{PLC\delta}$ or GFP-PH$^{PLC\delta}$, green) and specified actomyosin contractility regulators (magenta). (B-E) Same as in (C) but for a single confocal slice instead of a sum projection for animals expressing mNG::ANI-1 (B), NMY-2::GFP (C), GFP::ZEN-4 (D) and mNG::CYK-4 (E). The three graphs on the right report the fluorescence intensity of membrane (green) or contractility regulator (magenta) signal measured along each dotted line (1-3) drawn in the image on the left. Intensity peaks of contractility regulators define bridge diameter (black lines and arrows). In all panels, scale bar = 3μm.

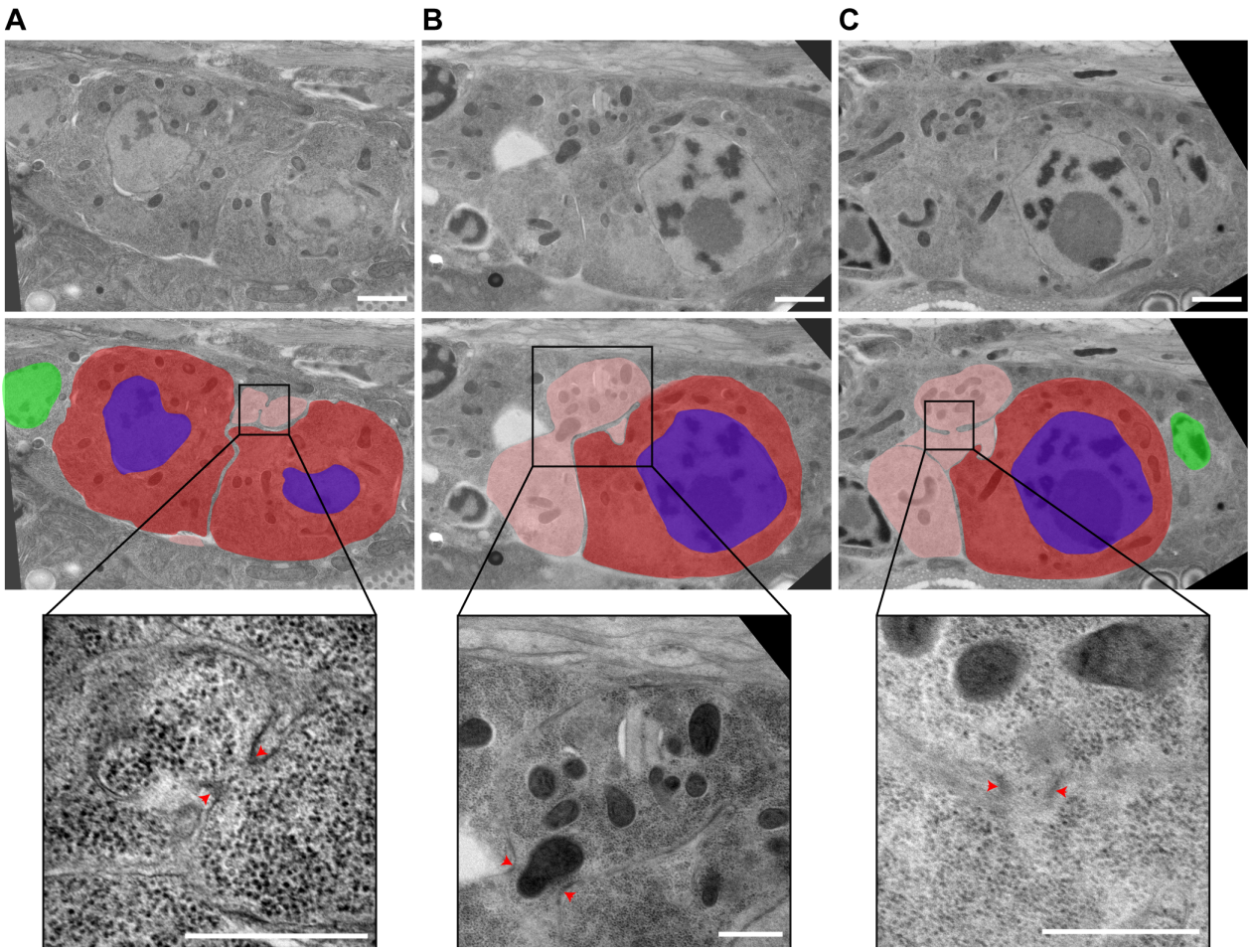

Fig. S3. (A-C) Selected TEM images from 90 nm-thick sections of the primordial germ line from a first larval stage animal. The middle panel is a color-overlayed version of the top panel, depicting nuclei (blue), PGC cytoplasm (dark red) and cytoplasm within the membrane-dense structure between the PGCs (light red). Scale bar = 1 µm. Insets at the bottom are magnifications of the boxed regions in the middle panels, where cytoplasmic bridges are visible within the membrane-dense structure (red arrowheads), possibly at the base of membrane lobes. The nuclei of the somatic primordial gonad (Z_1 and Z_4) are depicted in green. Scale bar = 500 nm.

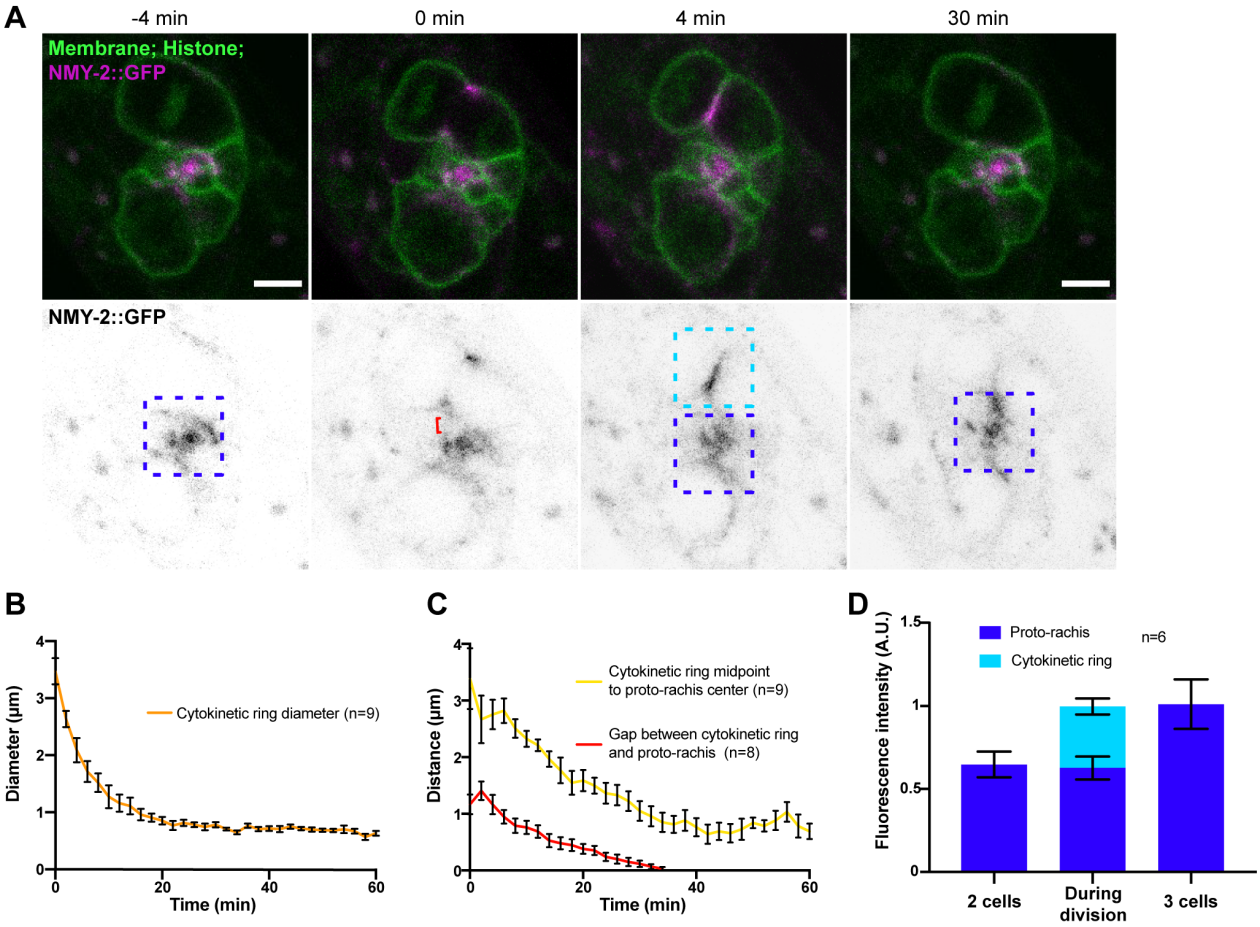

Fig. S4. (A) Confocal time-lapse images (sum projection of 3 slices) of PGCs undergoing first division in animals co-expressing markers for membrane and chromatin (TagRFP-PH$^{PLC\delta}$ & mCh-HIS-58, green) and NMY-2::GFP (magenta & bottom panels). The boxes indicate regions where fluorescence intensity was measured at the cytokinetic ring (light blue) and proto-rachis (dark blue) at the specified stages of cytokinesis. The bracket (red) indicates the gap between the cytokinetic ring and the proto-rachis. Time 0 is the onset of cytokinetic ring ingression. Scale bar = 3µm. (B-C) Measures of cytokinetic ring diameter (B; n = 9) and distance between the cytokinetic ring midpoint and the center of the proto-rachis (yellow line; n = 9) or the gap between the cytokinetic ring and the proto-rachis (red line; n = 8; C) over time in animals imaged as in (A). Error bars represent standard error of the mean. (D) Mean levels of NMY-2::GFP sum fluorescence intensity measured at the proto-rachis (dark blue) and cytokinetic ring (light blue, as depicted in A) before (2 cells), during and after (3 cells) PGC division. Error bars represent standard error of the mean, n = 6.

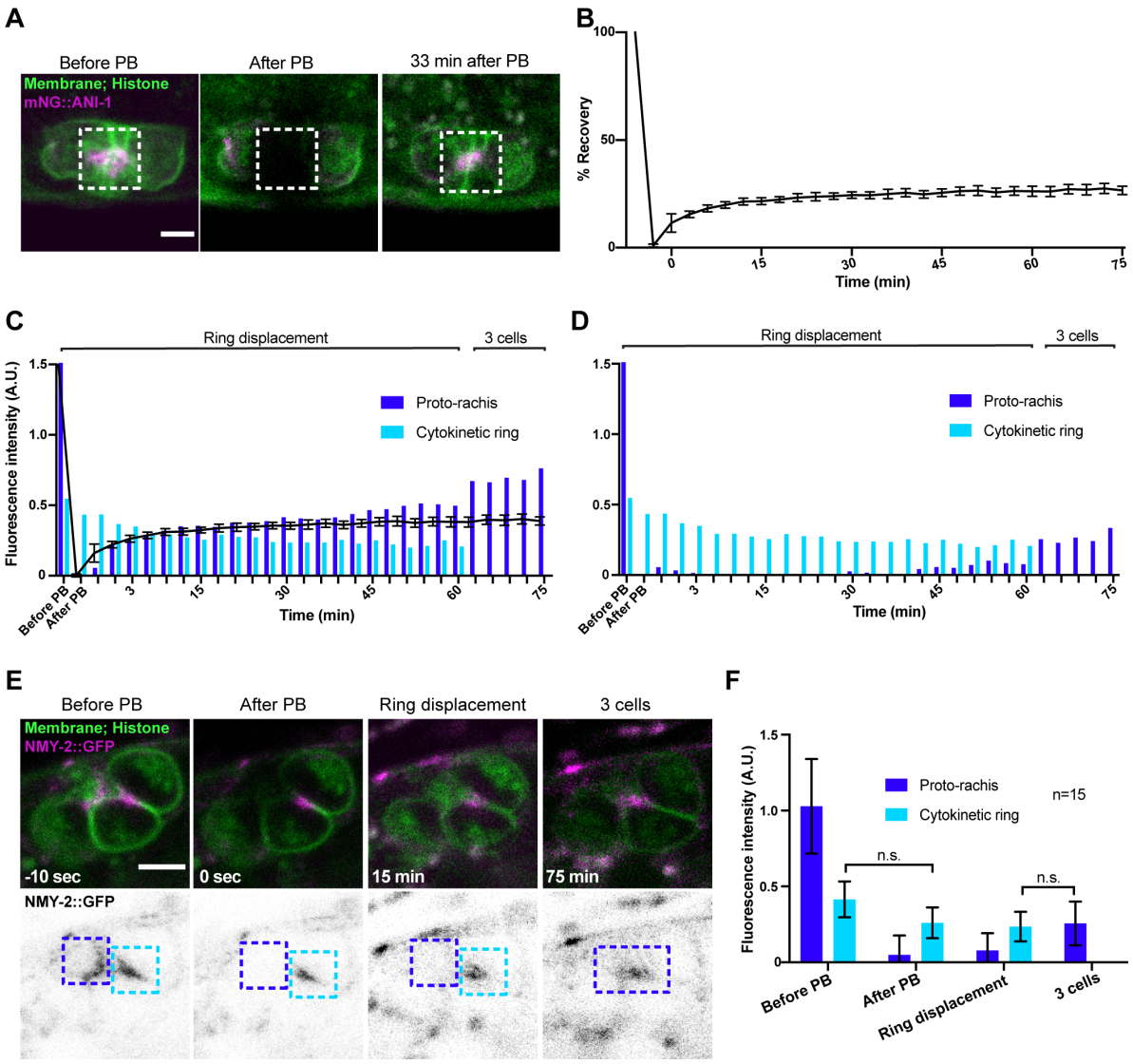

Fig. S5. (A) Confocal time-lapse images (sum projection of 3 slices) of non-dividing (mitotically quiescent) PGCs in animals co-expressing markers for membrane and chromatin (TagRFP-PH$^{PLC\delta}$ & mCh-HIS-58, green) and mNG::ANI-1 (magenta), taken before and after photobleaching (PB) of the signal at the proto-rachis (time 0). The boxes indicate regions where fluorescence intensity was measured at the proto-rachis over time. (B) Mean percentage of mNG::ANI-1 fluorescence recovery after photobleaching (FRAP) measured at the proto-rachis (as depicted in A). Error bars are standard error of the mean, n = 8 animals. (C-D) Mean levels of mNG::ANI-1 sum fluorescence intensity measured at the proto-rachis (dark blue) and cytokinetic ring (light blue, as depicted in Figure 3G) before and after photobleaching (PB) of the signal at the proto-rachis. The percent mNG::ANI-1 FRAP measured in B is overlayed in panel C and panel D represents the values at each timepoint after subtraction of these relative FRAP levels are subtracted from the measured fluorescence levels at the proto-rachis, thus effectively correcting for FRAP. (E) Confocal time-lapse images (sum projection of 3 slices) of PGCs undergoing first division in animals co-expressing markers for membrane and chromatin (TagRFP-PH$^{PLC\delta}$ & mCh-HIS-58, green) and NMY-2::GFP (magenta & bottom panels), taken before and after photobleaching (PB) of the signal at the proto-rachis (time 0). The boxes indicate regions where fluorescence intensity was measured at the cytokinetic ring (light blue) and proto-rachis (dark blue) over time. (F) Mean bleach-corrected levels of GFP::NMY-2 sum fluorescence intensity measured at the proto-rachis (dark blue) and cytokinetic ring (light blue, as depicted in E) before and after photobleaching (PB) of the signal at the proto-rachis. Error bars are standard error of the mean, n = 15 animals. Statistical analyses were done using an ordinary one-way ANOVA test with a Tukey post hoc test (ns = not significant, $p > 0.12$). In all panels, scale bar = 3μm.

Table S1. Strains used in this study

Strain	Genotype	Allele Reference
N2	Wild type	2
UM208	*unc-119(ed3) III; ltIs81[Ppie-1::gfp-tev-Stag::ani-2; unc-119(+)]; ltIs44[Ppie-1::mCherry::PH(PLC1delta1); unc-119(+)]*	1, 8
UM463	*cpIs42[Pmex-5::mNeonGreen::PLCδ-PH::tbb-2 3'UTR; unc-119(+)] II; ltIs37[pAA64; Ppie-1::mCherry::HIS-58; unc-119(+)] IV*	7, 11
UM639	*cpSi20[Pmex-5::TAGRFPT::PH::tbb-2 3'UTR; unc-119(+)] II; zuIs45[Pnmy-2::nmy-2::GFP; unc-119(+)]; ltIs37 [pAA64; Ppie-1::mCherry::HIS-58; unc-119(+)] IV*	7, 11, 12
UM641	*cpSi20[Pmex-5::TAGRFPT::PH::tbb-2 3'UTR; unc-119 (+)] II; ani-1(mon7[mNeonGreen^3xFlag::ani-1]) III; unc-119 (ed3) III*	7, 13
UM655	*cpSi20[Pmex-5::TAGRFPT::PH::tbb-2 3'UTR; unc-119 (+)] II; ani-1(mon7[mNeonGreen^3xFlag::ani-1]) III; unc-119(ed3)* III; ltIs37 [pAA64; Ppie-1::mCherry::HIS-58; unc-119(+)] IV*	7, 11, 13
UM717	*cp52[nmy-2::mkate2 + LoxP unc-119(+) LoxP] I; ccm-3(mon9[ccm-3::mNeonGreen^3xFlag]) II; unc-119(ed3)* III; ltIs44[pAA173, Ppie-1::mCherry::PH(PLC1delta1); unc-119(+)]*	4, 8, 13
UM735	*xnSi1[Pmex-5::GFP::PH(PLC1delta1)::nos-2 3'UTR] II; estSi71[pAC257;Pmex-5::lifeAct::mKate2::tbb-2 3'UTR; cb-unc-119(+)] IV*	3, 10
UM740	*cpSi20[Pmex-5::TAGRFPT::PH::tbb-2 3'UTR; unc-119 (+)] II; ltIs37 [pAA64; Ppie-1::mCherry::HIS-58; unc-119(+)] IV; ltIs154 [pOD539(pBG3); Ppie-1::cyk-7::GFP; unc-119 (+)]*	5, 7, 11
UM785	*axIs1959[Ppie-1::Dendra2::TEV::S-peptide::pie-1 3'UTR; unc-119(+)]; ani-1(mon7[mNeonGreen^3xFlag::ani-1]) III; unc-119(ed3)* III; ojIs1[Ppie-1::GFP::tbb-2; unc-119(+)] V*	6, 13, 14
OD3840	*ltSi849[pKL120; Pmex-5::mCherry::PH(PLC1delta1)::tbb-2 3'UTR; cb-unc-119(+)] I; unc-119(ed3)* III; zen-4(lt30[GFP::loxP::zen-4]) IV*	9
OD3686	*ltSi849[pKL120; Pmex-5::mCherry::PH(PLC1delta1)::tbb-2 3'UTR; cb-unc-119(+)] I; ltSi1124[pSG092; Pcyk-4::CYK- 4reencoded::mNeonGreen::cyk-4 3'-UTR; cb- unc-119(+)] II; unc- 119(ed3) III*	9

* *unc-119(ed3)* was in the parental strain but may not be present in this strain.

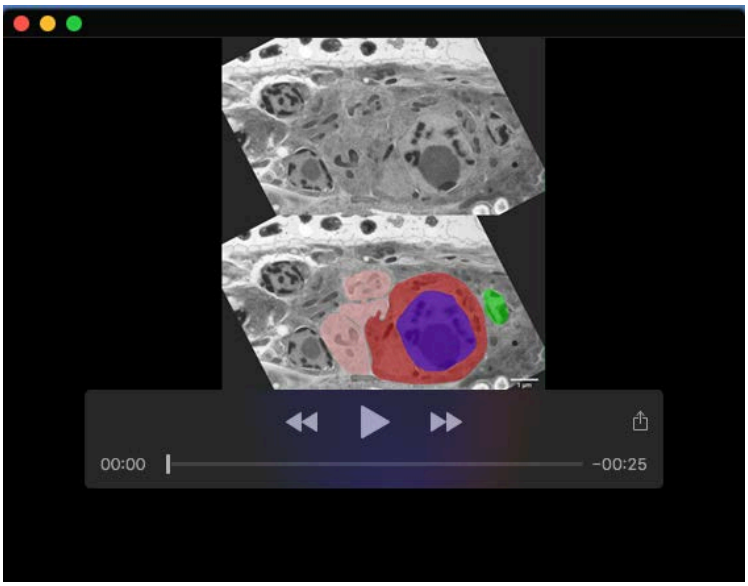

Movie 1. Serial transmission electron microscopy images from 90 nm-thick sections of the primordial germ line from a first larval stage animal. The bottom panel is a color-overlayed version of the top panel, depicting nuclei (blue), PGC cytoplasm (dark red) and cytoplasm within the membrane-dense structure between the PGCs (i.e. the proto-rachis, light red). The nuclei of the somatic primordial gonad (Z_1 and Z_4) are depicted in green. Images were aligned manually.

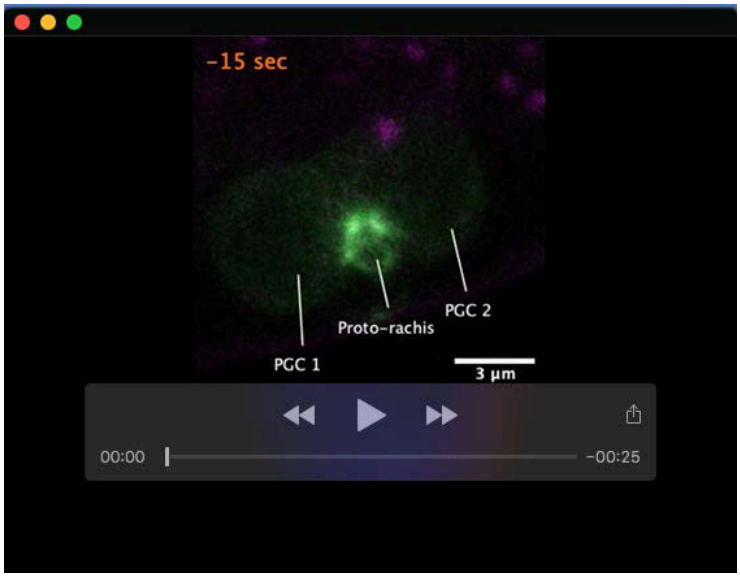

Movie 2. Time-lapse movie of the primordial germ line with two mitotically quiescent PGCs before and after Dendra2 fluorescence photoconversion (same images as shown in figure 1F), in animals co-expressing mNG::ANI-1 and cytoplasmic Dendra2. Images were acquired every 15 sec and are played at 1 frame per sec.

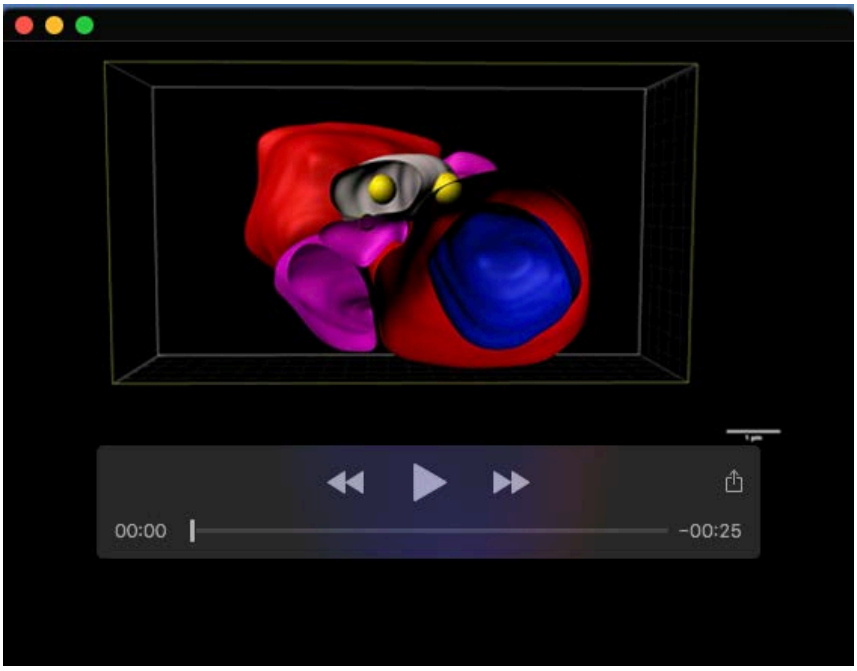

Movie 3. Tridimensional rendering of the primordial germ line displaying the proto-rachis (white compartment), to which both PGCs (red, with nuclei in blue) and membrane lobes (magenta) are connected via intercellular bridges (yellow spheres). This rendering was made from reconstructed EM images. Each image was imported into Inkscape software (v1.1) and the membrane defining each compartment was manually traced. To make intercellular bridges more visible, each was defined as a yellow sphere with a diameter equal to that of the bridge. Each compartment was then filled with colour in separate channels (1 channel per colour) and saved as a tif file. The file was imported into Imaris software (v9.2.1, Bitplane) and the "surface" tool was used to generate a 3D rendering of each defined compartment in each slice. The "clipping plane" tool was used to generate a composite image of each slice and these composite images were assembled with ImageJ software into a movie that sequentially goes from the bottom to the top of the primordial germ line. The "animation" tool from Imaris software was used to rotate the entire reconstructed 3D image.

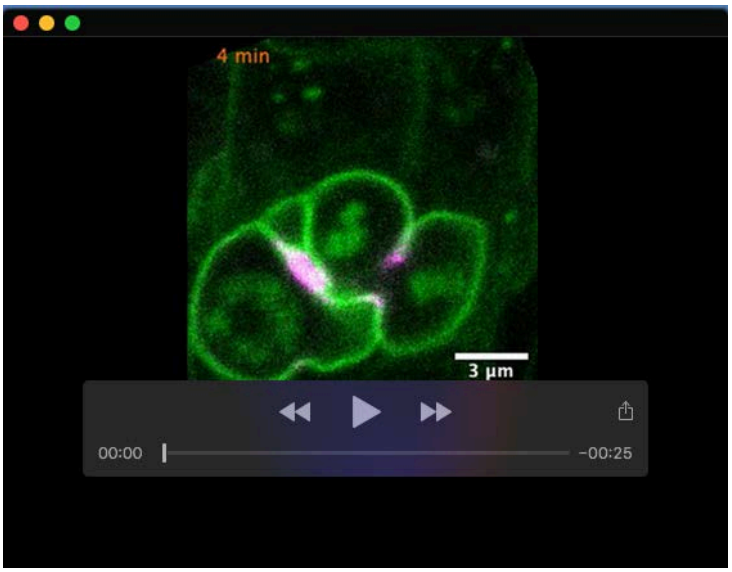

Movie 4. Time-lapse movie of the first division of the PGCs (same images as shown in figure 3C), in animals co-expressing mNG::ANI-1, a membrane (TagRFP::PH) and a histone (mCherry::HIS-58) marker. Images were acquired every 2 min and are played at 3 frames per sec.

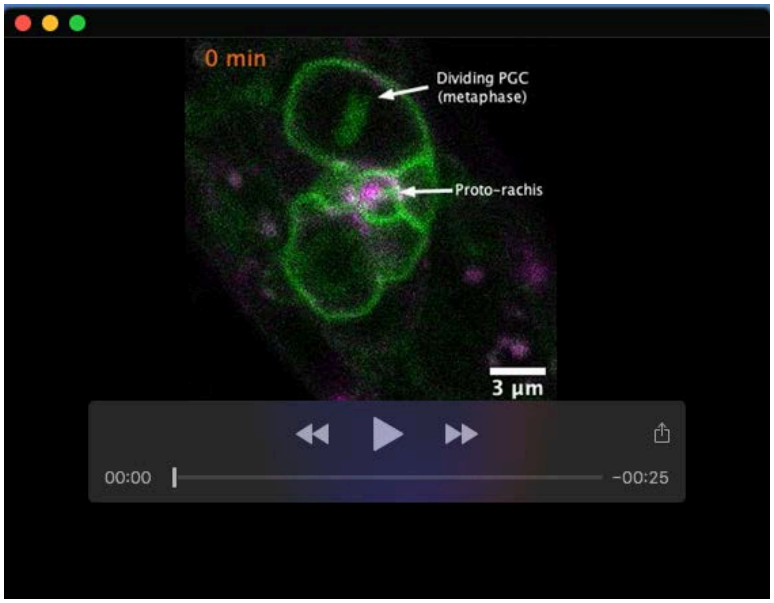

Movie 5. Time-lapse movie of the first division of the PGCs (same images as shown in figure S4A), in animals co-expressing NMY-2::GFP, a membrane (TagRFP::PH) and a histone (mCherry::HIS-58) marker. Images were acquired every 2 min and are played 3 frames per sec.

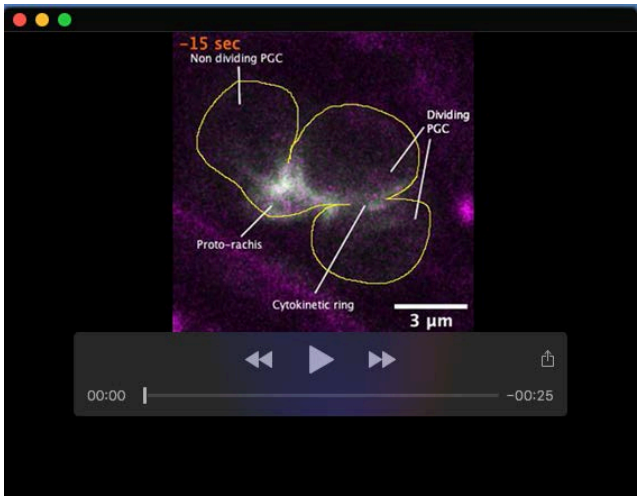

Movie 6. Time-lapse movie of the primordial germ line with one PGC undergoing cytokinesis before and after Dendra2 fluorescence photoconversion (same images as shown in figure 4B), in animals co-expressing mNG::ANI-1 and cytoplasmic Dendra2. Images were acquired every 15 sec and are played at 1 frame per sec.

Supplemental References

1. **Amini, R., Goupil, E., Labella, S., Zetka, M., Maddox, A. S., Labbé, J. C. and Chartier, N. T.** (2014). *C. elegans* Anillin proteins regulate intercellular bridge stability and germline syncytial organization. *J Cell Biol* **206**, 129-143.
2. **Brenner, S.** (1974). The genetics of *Caenorhabditis elegans*. *Genetics* **77**, 71-94.
3. **Chihara, D. and Nance, J.** (2012). An E-cadherin-mediated hitchhiking mechanism for *C. elegans* germ cell internalization during gastrulation. *Development* **139**, 2547-2556.
4. **Dickinson, D. J., Schwager, F., Pintard, L., Gotta, M. and Goldstein, B.** (2017). A Single-Cell Biochemistry Approach Reveals PAR Complex Dynamics during Cell Polarization. *Dev Cell* **42**, 416-434 e411.
5. **Green, R. A., Kao, H. L., Audhya, A., Arur, S., Mayers, J. R., Fridolfsson, H. N., Schulman, M., Schloissnig, S., Niessen, S., Laband, K., et al.** (2011). A high-resolution *C. elegans* essential gene network based on phenotypic profiling of a complex tissue. *Cell* **145**, 470-482.
6. **Griffin, E. E., Odde, D. J. and Seydoux, G.** (2011). Regulation of the MEX-5 gradient by a spatially segregated kinase/phosphatase cycle. *Cell* **146**, 955-968.

7. **Heppert, J. K., Dickinson, D. J., Pani, A. M., Higgins, C. D., Steward, A., Ahringer, J., Kuhn, J. R. and Goldstein, B.** (2016). Comparative assessment of fluorescent proteins for in vivo imaging in an animal model system. *Mol Biol Cell* **27**, 3385-3394.
8. **Kachur, T. M., Audhya, A. and Pilgrim, D. B.** (2008). UNC-45 is required for NMY-2 contractile function in early embryonic polarity establishment and germline cellularization in *C. elegans*. *Dev Biol* **314**, 287-299.
9. **Lee, K. Y., Green, R. A., Gutierrez, E., Gomez-Cavazos, J. S., Kolotuev, I., Wang, S., Desai, A., Groisman, A. and Oegema, K.** (2018). CYK-4 functions independently of its centralspindlin partner ZEN-4 to cellularize oocytes in germline syncytia. *Elife* **7**.
10. **Mangal, S., Sacher, J., Kim, T., Osorio, D. S., Motegi, F., Carvalho, A. X., Oegema, K. and Zanin, E.** (2018). TPXL-1 activates Aurora A to clear contractile ring components from the polar cortex during cytokinesis. *J Cell Biol* **217**, 837-848.
11. **McNally, K., Audhya, A., Oegema, K. and McNally, F. J.** (2006). Katanin controls mitotic and meiotic spindle length. *J Cell Biol* **175**, 881-891.
12. **Nance, J., Munro, E. M. and Priess, J. R.** (2003). *C. elegans* PAR-3 and PAR-6 are required for apicobasal asymmetries associated with cell adhesion and gastrulation. *Development* **130**, 5339-5350.
13. **Rehain-Bell, K., Love, A., Werner, M. E., MacLeod, I., Yates, J. R., 3rd and Maddox, A. S.** (2017). A Sterile 20 Family Kinase and Its Co-factor CCM-3 Regulate Contractile Ring Proteins on Germline Intercellular Bridges. *Curr Biol* **27**, 860-867.
14. **Strome, S., Powers, J., Dunn, M., Reese, K., Malone, C. J., White, J., Seydoux, G. and Saxton, W.** (2001). Spindle dynamics and the role of gamma-tubulin in early *Caenorhabditis elegans* embryos. *Mol Biol Cell* **12**, 1751-1764.